

Subharmonic excitation in amplitude modulation atomic force microscopy in the presence of adsorbed water layers

Sergio Santos, Victor Barcons, Albert Verdaguer, and Matteo Chiesa

Citation: *J. Appl. Phys.* **110**, 114902 (2011); doi: 10.1063/1.3663437

View online: <http://dx.doi.org/10.1063/1.3663437>

View Table of Contents: <http://jap.aip.org/resource/1/JAPIAU/v110/i11>

Published by the [American Institute of Physics](http://www.aip.org).

Related Articles

Large and stable piezoelectric response in Bi_{0.97}Nd_{0.03}FeO₃ thin film

Appl. Phys. Lett. **100**, 172904 (2012)

Imaging of subatomic electron cloud interactions: Effect of higher harmonics processing in noncontact atomic force microscopy

Appl. Phys. Lett. **100**, 163104 (2012)

Qualitative determination of surface roughness by in situ reflection high energy electron diffraction

Appl. Phys. Lett. **100**, 151604 (2012)

Local resistive switching of Nd doped BiFeO₃ thin films

Appl. Phys. Lett. **100**, 133505 (2012)

Al doped Ba hexaferrite (BaAl_xFe_{12-x}O₁₉) thin films on Pt using metallo-organic decomposition

J. Appl. Phys. **111**, 07A514 (2012)

Additional information on J. Appl. Phys.

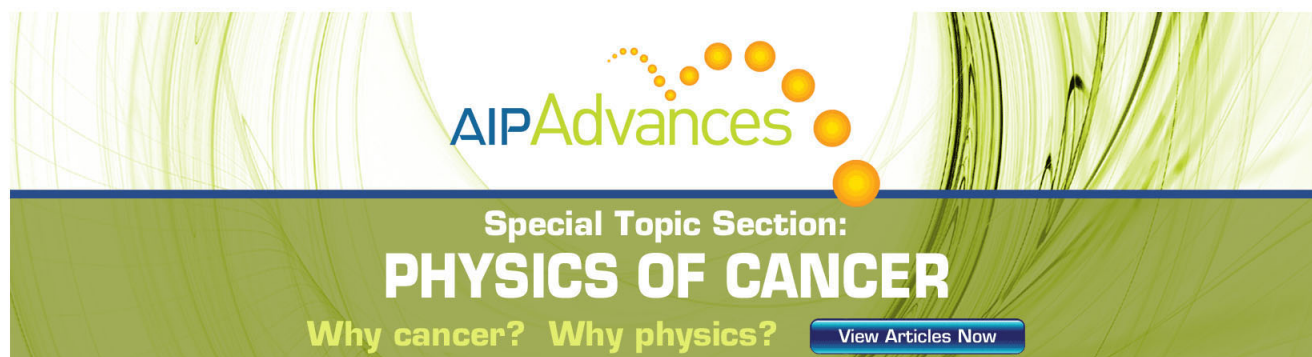
Journal Homepage: <http://jap.aip.org/>

Journal Information: http://jap.aip.org/about/about_the_journal

Top downloads: http://jap.aip.org/features/most_downloaded

Information for Authors: <http://jap.aip.org/authors>

ADVERTISEMENT



AIP Advances

Special Topic Section:
PHYSICS OF CANCER

Why cancer? Why physics? [View Articles Now](#)

Subharmonic excitation in amplitude modulation atomic force microscopy in the presence of adsorbed water layers

Sergio Santos,¹ Victor Barcons,² Albert Verdaguer,³ and Matteo Chiesa^{1,4,a)}

¹Laboratory of Energy and Nanosciences, Masdar Institute of Science and Technology, P.O. BOX 54224, Abu Dhabi, United Arab Emirates

²Departament de Disseny i Programació de Sistemes Electrònics, UPC - Universitat Politècnica de Catalunya Av. Bases, 61, 08242 Manresa, Spain

³Centre d' Investigació en Nanociència i Nanotecnologia (CIN2) (CSIC-ICN), Esfera UAB, Campus de la UAB, Edifici CM-7, 08193-Bellaterra, Catalunya, Spain

⁴Department of Mechanical Engineering, Massachusetts Institute of Technology, 77 Massachusetts Avenue, Cambridge, Massachusetts 02139-4307, USA

(Received 8 July 2011; accepted 26 October 2011; published online 2 December 2011)

In ambient conditions, nanometric water layers form on hydrophilic surfaces covering them and significantly changing their properties and characteristics. Here we report the excitation of subharmonics in amplitude modulation atomic force microscopy induced by intermittent water contacts. Our simulations show that there are several regimes of operation depending on whether there is perturbation of water layers. Single period orbitals, where subharmonics are never induced, follow only when the tip is either in permanent contact with the water layers or in pure noncontact where the water layers are never perturbed. When the water layers are perturbed subharmonic excitation increases with decreasing oscillation amplitude. We derive an analytical expression which establishes whether water perturbations compromise harmonic motion and show that the predictions are in agreement with numerical simulations. Empirical validation of our interpretation is provided by the observation of a range of values for apparent height of water layers when subharmonic excitation is predicted. © 2011 American Institute of Physics. [doi:10.1063/1.3663437]

I. INTRODUCTION

Part of the interest in measuring surface features with nanometric and subnanometric resolution lies in the fact that dimension is one of the fundamental characteristics at the nanoscale.^{1,2} The size of a nanoscale object is closely linked to properties such as electronic energy levels and surface to volume ratio, thus directly affecting electrical and optical properties, adhesion, chemical reactivity and cohesion. In particular, nanoscale research is interested in the properties of surfaces since it is mostly via the surface that systems interact. Thus, it is not surprising that much effort is being put to understand nanoscale phenomena on surfaces.^{3–6}

The atomic force microscope (AFM) is a particularly suitable instrument to study surfaces with nanoscale resolution.^{3,7} The AFM consists of a microcantilever with a sharp tip at its end which is brought into proximity with surfaces in order to monitor the interactions. In the dynamic modes, the cantilever is oscillated at or close to its resonance frequency and the tip intermittently interacts with the surface via surface forces. This provides a means to understand phenomena occurring in the tip-sample junction in a dynamic fashion.⁸ Several groups have been investigating the dynamics of the instrument since its invention.^{9–20}

In ambient conditions, there is typically a nanometer thick layer of water on surfaces.²¹ As a result, at small tip-surface separations, capillary interactions can have a significant effect

on the dynamics of the cantilever.²² Some have reported no particular effect on the linearity of the oscillation amplitude under the influence of capillary forces.²³ Others have theoretically shown how the nonlinearities introduced by capillary interactions can lead to the appearance of several attractors.²² Capillary effects have also been reported to be responsible for energy dissipation maps in hydrophobic/hydrophilic interactions.²⁴ Still, others²⁵ have reported that the interaction with water layers can be predicted by analyzing the mean deflection of the cantilever, where a small jump in deflection should be expected when water interactions occur. The AFM has also been used to verify a decrease in adhesion force with increasing relative humidity²⁶ and to quantify an effective water stiffness for nanometric water columns.²⁷ Furthermore, since some forms of AFM, such as Kelvin probe (KP) AFM, rely on a pure non-contact mode of operation, much effort has been put to understand this phenomenon. Partly, the interest of so many groups in the role of capillary interactions at the nanoscale lies in the implications of hydration on surface properties and reactivity. For example, nanoscale hydration may affect macroscale phenomena with implications in corrosion, direct or galvanic currents, ion flow on surfaces, and the catalysis of surface reactions.^{5,6,28}

Here we describe the dynamics of the cantilever in amplitude modulation (AM) AFM in hydrated environments where nanometer thick water layers cover the surfaces. Our study focuses on surfaces that are exposed to humidity in otherwise ambient conditions. We show that according to simulations a discrete negative jump in mean cantilever deflection does not relate to water intermittent perturbation but to perpetual contact between the tip and the water layers.

^{a)}Author to whom correspondence should be addressed. Electronic address: mchiesa@mit.edu.

Intermittent contact with the water might occur before the discrete jump. When the tip is inside the water layer and in perpetual contact with it, a unique limit cycle is predicted which consists of a single period orbital. When intermittent contact occurs and the capillary bridge is formed and ruptured during an oscillation cycle, the steady state with constant oscillation amplitude cannot be reached since the limit cycle displays multiple period orbitals. The oscillations are then modulated by frequencies that can be an order of magnitude smaller than the fundamental or drive frequency. This behavior can be observed in the simulations by analyzing the wave form or by noting the appearance of subharmonics in the motion. The physical interpretation is that the tip is perturbed by capillary neck formation with frequencies which are smaller than the fundamental but still in the range of microseconds. The appearance of subharmonics thus might provide the means to investigate the time scale for the nucleation of water bridges in the nanoscale. Since the understanding of time scale for these processes is still emerging,^{24,29,30} our method could provide insight into such investigations. We demonstrate with simulations and also experimentally the effects of water perturbation on apparent height measurements. Large errors in apparent height measurements of water layers are observed when multiple period orbitals and subharmonics are predicted. We further show that with increasing oscillation amplitude, the effects of water perturbations are reduced in terms of the multiple period orbitals range. Physically, this implies that the ratio between the magnitude of water perturbations and the elastic response of the cantilever tends to zero with increasing oscillation amplitude. Finally, we show that in the repulsive regime, where intermittent mechanical contact occurs, experimental nonzero apparent height measurements of water layers are obtained. These nonzero heights can be reproduced in simulations if we assume, as suggested in previous studies,³¹ that one or several water layers remain when mechanical indentation of the surface occurs. In our model, we account for the atoms in the water films on both the tip and the surface by considering their effect on the long range van der Waals force. We also consider the effects on adhesion that these atoms have when the capillary neck is formed.

II. MODEL AND METHODS

The equation of a damped driven harmonic oscillator³² (1) with the addition of the tip-surface forces F_{ts} (2) is used where F_{ts} is the net tip-surface force. For the particular forces acting we use subscripts (2). This model is a good approximation to the real phenomenon in ambient conditions where the Q factor is relatively high³³ (i.e., $Q \sim 10^2$ – 10^3). That is, under these conditions, the contributions of the second mode can be neglected. The fundamental tip-surface distance dependencies are shown in a scheme in Fig. 1

$$m \frac{d^2 z}{dt^2} + \frac{m \omega_0}{Q} \frac{dz}{dt} + kz = F_{ts} + F_0 \cos \omega t, \quad (1)$$

$$F_{ts}(d) = F_{vdW} + F_{CAP} + F_{AD} + F_{DMT}. \quad (2)$$

Here the spring constant of the cantilever is k , the natural angular frequency is ω_0 , the effective mass of the tip is³²

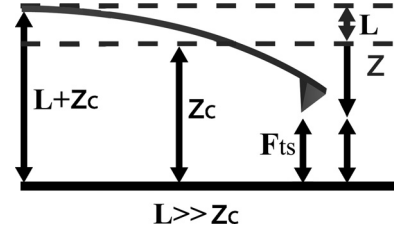


FIG. 1. Scheme where some of the distance dependencies between the tip, the cantilever and the surface are shown. Here z_c is the tip-surface equilibrium separation, z is the instantaneous position of the tip relative to z_c and d is the distance to the solid surface, that is, the surface if there was no water. L is the distance between the tip and the cantilever. This distance is typically orders of magnitude larger than z_c . Thus, L is not required to model the equation of motion. The tip-surface distance d is defined as $z_c + z$ where negative values for z are taken in the downward direction. The distance dependencies for the tip-surface force F_{ts} are calculated with d . The parameters that have physical significance for an understanding of the dynamics are z_c , z , d , and F_{ts} . Dependencies when the capillary force are taken into account are shown in Fig. 2.

$m = k/(\omega_0)^2$ and the driving force is $F_0 \cos \omega t$. We use the following expressions for the van der Waals (vdW) (F_{vdW}), the capillary (F_{CAP}),³⁴ the adhesion (F_{AD}), and the repulsive forces (F_{DMT})³⁵

$$F_{vdW}(d^*) = -\frac{H_{H_2O} R}{6(d^*)^2} \quad \text{noncontact}, \quad (3)$$

$$F_{AD}(H^*) = -\frac{H_s^* R}{6a_0^2} \quad \text{water contact}, \quad (4)$$

$$F_{CAP}(d) = -C \left(\frac{2\pi\gamma_{H_2O} R}{1 + \frac{\pi R d^2}{V_{men}}} \right) \quad \text{water contact}, \quad (5)$$

$$F_{AD} = -\frac{H_s R}{6a_0^2} \quad \text{mechanical contact}, \quad (6)$$

$$F_{CAP}(d) = -C \left(\frac{2\pi\gamma_{H_2O} R}{1 + \frac{\pi R a_0^2}{V_{men}}} \right) \quad \text{mechanical contact}, \quad (7)$$

$$F_{DMT}(d) = \frac{4}{3} E^* \sqrt{R(a_0 - d)^3} \quad \text{mechanical contact}. \quad (8)$$

Here a_0 is an intermolecular distance which implies that matter interpenetration can never occur.⁶ In Eqs. (3)–(8) the tip is modeled as a sphere with curvature R . In the tip-surface interaction we account for the long range vdW forces between a sphere and an infinite plane³⁶ but the effect of the water layer is also accounted for by taking into account an effective distance of interaction d^* . Thus, in Eq. (3) H_{H_2O} is the effective Hamaker³⁶ for the hydrated tip-surface pair at a distance $d^* = d - 2h$ [Fig. 2(a)].³⁷ This is the long range force and accounts for the long range noncontact interactions of the atoms in the solid systems and also in the water films. When the capillary bridge is formed [Fig. 2(b)], an adhesive component due to the water-water interactions from the tip and the surface

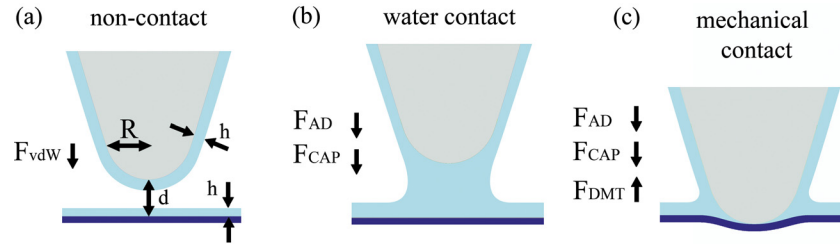


FIG. 2. (Color online) Scheme of the three possibilities for a hydrated tip interacting with a hydrated surface. (a) The first possibility involves a purely noncontact interaction. Here only long range forces such as the van der Waals (vdW) act. (b) The second possibility involves the tip and the water layers on it interacting with the water layers on the surface. (c) In the third possibility the tip indents the surface and mechanical contact occurs. The water layers are only perturbed in the second and third cases. The acting forces in each case are indicated in the schemes.

appears. This is F_{AD} (4), and because contact between the water layers is made already in this case, there is no explicit distance dependency, i.e., $d^* = a_0$. Nevertheless, the Hamaker constant still has a distance dependency since the atoms on the water layers on the tip and the surface and the atoms on the solid tip and the solid surface are involved in this interaction. Thus, we interpolate the Hamaker constant value and write H^* from the point at which the capillary is formed until mechanical contact is made. Mechanical contact occurs at $d = a_0$ (see supplementary material for details⁵²). Of course, at this point the capillary force³⁴ (5) also acts. However, we multiply the capillary force by a constant C which implies that the capillary interaction is reduced experimentally relative to the expression inside the brackets. This is because asperities in the tip are not accounted for in the derivations of this equation.^{6,34} We have used $C = 0.5$ in our simulations. Also, γ_{H_2O} is the surface energy of water and V_{men} is the volume of the meniscus which can be obtained from geometrical considerations.²³ In a third stage [Fig. 2(c)] mechanical contact occurs. At this point the Hamaker constant is simply H_s for the solid tip-surface pair and the adhesive component (6) is constant.³⁵ In the contact region, we also saturate the capillary force in terms of distance (7) but allow for the volume to grow with increasing indentation²³ (see supplementary material for details⁵²). The main force addition here is the repulsive force (8) from the Derjaguin-Muller-Toporov (DMT) model of contact mechanics.³⁵

We have implemented this model in both Matlab and C. While both codes produced identical results, the model implemented in C is computationally superior. We have employed a standard Runge Kutta Algorithm of the fourth order and compared it with fifth and eighth order Runge Kutta algorithms and with the Adams-Bashforth algorithm of the fourth order without significant improvement in the simulations. Our experimental work was carried out on an Asylum Research Cypher and on an Asylum Research MFP-3 D-SA AFM working at the natural frequency of oscillation. We have performed experiments on mica surfaces and on a BaF₂(111) surface where water molecules can form well defined water patches.³¹ Finally, in our experiments, we have stabilized the tips prior to obtaining our data by submitting them to ever increasing forces from initial small attractive forces. We have previously^{38,39} described this procedure in detail and shown that it can lead to tip stability and reproducibility in terms of the dynamics of the cantilever.

III. RESULTS AND DISCUSSION

A. The analytic expression for stability and its consequences

We start by establishing the parameters for stability and harmonic motion analytically. The net work done by the capillary force during one period depends on the magnitude of the capillary force, the hysteresis in capillary formation and rupture, i.e., $d_{off} - d_{on}$, and the difference in adhesion on approach and retraction (3) and (4). Here d_{on} is the distance at which the capillary forms on approach and d_{off} is the distance at which the capillary ruptures on retraction. Furthermore $d_{off} > d_{on}$.²³ For compactness we write Eq. (5) in the form

$$F_{CAP}(d) = -\theta(C, R, \gamma_{H_2O})\Gamma(V_{men}, R, d), \quad (9)$$

where

$$\theta = 2\pi\gamma_{H_2O}CR, \quad (10)$$

$$\Gamma = \frac{1}{1 + (Bd)^2}, \quad (11)$$

and

$$B = \left(\frac{\pi R}{V_{men}}\right)^{1/2}. \quad (12)$$

Here, θ (10) accounts for geometrical characteristics such as tip radius R , possible asperities via C and chemistry via the surface energy of water γ_{H_2O} . We assume these to be constant in the experiments. On the other hand, the distance dependencies are accounted for via the function Γ (11); this function also depends on R and the volume of the water meniscus V_{men} through B (12). Now we can find the work done by the capillary force by assuming a distance of minimum approach d_{min} where $d_{min} \leq d_{on}$. We are not interested in distances smaller than d_{on} because below this distance the capillary is always formed; here, we take $d_{on} = 3h$.^{6,34} Work is then done between d_{on} and d_{off} on retraction provided the capillary forms and ruptures during an oscillation cycle. This implies $d_{min} < d_{on}$ and $d_{max} > d_{off}$, where d_{max} is the maximum distance between the tip and the surface during an oscillation cycle. That is, the range of oscillation $d_{max} - d_{min}$ is required to be larger than the difference between d_{on} and d_{off} and also include this range.

Then, we write for the net work done by the capillary force in one cycle

$$W_{CAP} = \theta \int_{z=d_{on}}^{z=d_{off}} \Gamma(z) dz, \quad (13)$$

which gives

$$W_{CAP} = \frac{\theta}{B} [\tan^{-1}(Bd_{off}) - \tan^{-1}(Bd_{on})] \quad (14)$$

We interpret all work as positive and as representing energy dissipated in the interaction. We can also consider the work done by adhesion due to the hysteresis implied by Eqs. (3) and (4) since, as stated, Eq. (3) applies on approach and Eq. (4) on retraction when the capillary forms and ruptures in once cycle (see supplementary material for details⁵²). For this work we write

$$W_{AD} = \xi^1 (d_{off}^2 - d_{on}^2) + \xi^2 (d_{off} - d_{on}) - \xi^3 \left[\frac{1}{d_{on} - 2h} - \frac{1}{d_{off} - 2h} \right], \quad (15)$$

where, in order to make the expression compact, we have written

$$\xi^1 = \frac{\Delta HR}{12(d_{off} - a_0)a_0^2}, \quad \xi^2 = \frac{R}{6a_0^2} \left[H_S - \frac{\Delta H a_0}{(d_{off} - a_0)} \right],$$

$$\xi^3 = \frac{RH_{H_2O}}{6} \quad \text{and} \quad \Delta H = H_{H_2O} - H_S.$$

Moreover, since the energy dissipated due adhesion hysteresis in Eq. (15) also has to do with the onset of the capillary bridge, we can more compactly write W_{CAP} as the addition of Eqs. (14) and (15). In summary, W_{CAP} , i.e., Eqs. (14) + (15), is the energy that leaves the cantilever during one cycle when the capillary bridge is formed at a distance d_{on} and then ruptured at d_{off} . In this respect W_{CAP} can be thought of as a perturbation energy. If this perturbation energy is large compared to the stored energy in the cantilever, then, harmonic motion is compromised. This relationship can be written as a ratio

$$P = \frac{W_{CAP}}{E_c}, \quad (16)$$

where P stands for normalized perturbation energy and E_c is the energy stored in the cantilever. Furthermore, E_c can be simplified for harmonic motion and to a first approximation to³²

$$E_c \approx 1/2kA^2 \quad (17)$$

From Eqs. (16) and (17) we infer that stable oscillations in amplitude A , i.e., harmonic motion, should be compromised with decreasing oscillation amplitude and decreasing spring constant k provided the capillary forms and ruptures during one cycle, i.e., $d_{min} < d_{on}$ and $d_{max} > d_{off}$. The dependency of the volume of the water meniscus V_{men} on perturbations in Eq. (16) is accounted for by B (12). Of course the contributions of θ in Eq. (16) should not be ignored and these imply

that stability is compromised with increasing tip radius R and decreasing number or increasing size of asperities when the capillary is formed and ruptured. Recall that asperities are controlled by C in Eqs. (5) and (9). Nevertheless, if the asperities and the tip curvature, together with the water height or meniscus and k are assumed to be constant parameters in the experiments, then stability is controlled by A and d_{min} only. Thus, stability should decrease with decreasing A provided the capillary ruptures in one cycle, that is, provided d_{min} is sufficiently small as for the capillary bridge to be formed and provided d_{max} is sufficiently large as for the capillary bridge to rupture, i.e., $d_{min} < d_{on}$ and $d_{max} > d_{off}$. Note that this condition implies that if $d_{max} < d_{off}$ while the capillary is formed, that is, if there is perpetual water contact, perturbations should be minimized and in fact zero if the capillary is the only form of perturbation as in this study. In the next section we show with simulations that a limit cycle with a single period orbital follows under these conditions and that subharmonics are not excited.

B. Subharmonics and limit cycles

In Fig. 3(a) an experimental amplitude distance (AD) curve obtained on a mica surface at a relative humidity (RH) of 50–60% is shown. This curve has been obtained for a small value of A_0 , i.e., $A_0 = 3$ nm. The tip radius was estimated to be 10–20 nm in these experiments. AD curves are obtained by oscillating the cantilever at a given free amplitude A_0 while at or near resonance.⁴⁰ Here A_0 is defined as the amplitude of oscillation when the cantilever is unperturbed by surface forces; i.e., $z_c \gg A_0$. Then for the AD curve, the response of the oscillation amplitude A is monitored with decreasing separation z_c . Here, the amplitude and separation have been normalized as A/A_0 and z_c/A_0 , respectively. In experimental curves however, the zero value is chosen arbitrarily since this cannot be experimentally found in a trivial way.⁴¹ Approach to the surface and retraction from the surface are indicated by arrows in Fig. 3(a). Note that the amplitude for small separations coincides on approach and retraction. Nevertheless at larger separations, i.e., $z_c/A_0 \sim 1$, there is hysteresis on retraction. This behavior is reproduced in simulations in Fig. 3(b) for which the values $A_0 = 3$ nm and $R = 15$ nm have been used. The patterns during approach and retraction in the simulations are the same as the experimental ones. In Fig. 3(b) we differentiate regions where no water contact has occurred with continuous black lines. We term this region nc. Regions for which intermittent contact with water occurs are termed ic and these are shown with dashed black lines. In this case however, the only region where this occurs is where the tip either gets trapped or breaks free from the water. These are only transient phenomena in the curves. Finally, regions where perpetual water contact occurs during an oscillation cycle are shown in blue online and are termed pc standing for perpetual contact. The perpetual contact region is characterized by relatively large values of mean deflection (see Fig. 4 and discussion below). Perpetual contact implies that the water meniscus never ruptures during an oscillation cycle; i.e., $d_{max} < d_{off}$. Perpetual contact typically leads to negative

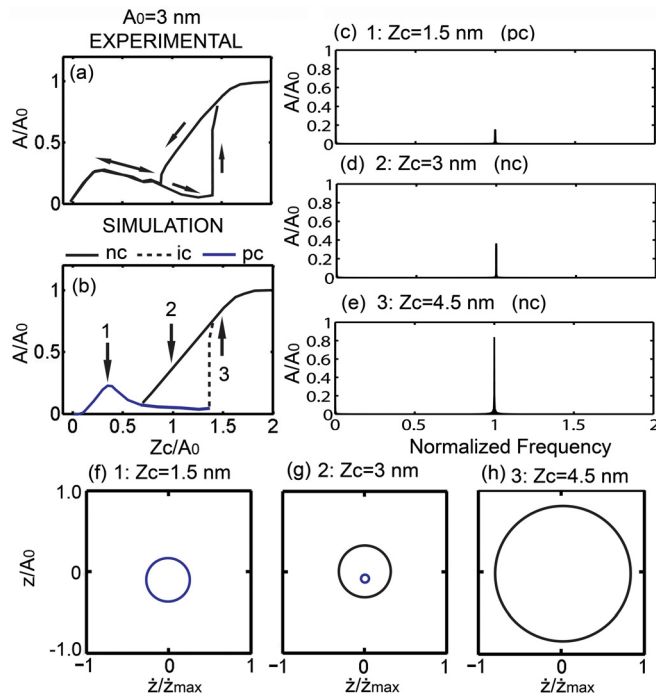


FIG. 3. (Color online) (a) Experimental amplitude distance (AD) curve obtained on a mica surface at a relative humidity (RH) of 50–60%. The arrows indicate the extension and retraction path. (b) Simulation of a similar curve where the experimental characteristics are reproduced. Here nc (continuous black lines), ic (dashed black lines), and pc (blue online) stand for pure noncontact, intermittent contact with water layers and perpetual contact with water layers. (c)–(e) Fast Fourier transforms FFTs obtained at three different separations z_c/A_0 as indicated by arrows in (b) and marked 1, 2, and 3, respectively. The horizontal axis has been normalized as f/f_0 where f_0 is the natural frequency. The vertical axis shows the normalized amplitudes A/A_0 . In (d) the FFT corresponds to the nc region in the curve. The figures show that neither the second harmonic nor subharmonics are excited. The respective phase space diagrams displaying the limit cycles of the system at each separation are shown in (f)–(h) respectively. These are all single period orbitals. The vertical axis is the normalized instantaneous position (see Fig. 1) and the horizontal axis shows the normalized instantaneous velocity. Experimentally, the average forces, i.e., the attractive and repulsive regimes, where monitored in (a) by recording the value of the phase lag where a net attractive force follows where the phase lag lies above 90 degrees.⁴³ Here the phase always lied above 90 degrees both in the experiments and in the simulations. Experimental parameters for (a): $f=f_0=270$ kHz, $k=35$ N/m, and $Q=400$ (quality factor). Simulation parameters: $f=f_0=270$ kHz, $k=35$ N/m, $R=15$ nm, $Q=400$, $\gamma=20$ mJ (surface energy of the surface), $\gamma_{H_2O}=72$ mJ (surface energy of water), $E=10$ GPa (elastic modulus of the surface⁴⁵), $E_t=120$ GPa (elastic modulus of the tip) and $h=0.6$ nm (water layer height).

mean deflection; conversely, the nc region (black continuous lines) has almost zero deflection (see Fig. 4). Considering that for the nc region in Fig. 3(b), $A_0=3$ nm, there is zero mean deflection, one can note that the minimum distance of approach in the nc region is ~ 2 nm in this case. This is consistent with nc since we have used $h=0.6$ nm and $d_{on}=3h=1.8$ nm. In Figs. 3(c)–3(e) we show the frequency response for the curve in Fig. 3(b). These have been obtained at three different separations as indicated by arrows in Fig. 3(b). The separations are (1) $z_c/A_0=0.5$ ($z_c=1.5$ nm), (2) $z_c/A_0=1.0$ ($z_c=3$ nm), and (3) $z_c/A_0=1.5$ ($z_c=4.5$ nm). Briefly, no subharmonics or higher harmonics are excited in any of these cases. This is consistent with the analytic expression (16) for stability since in all cases $W_{CAP}=0$. That

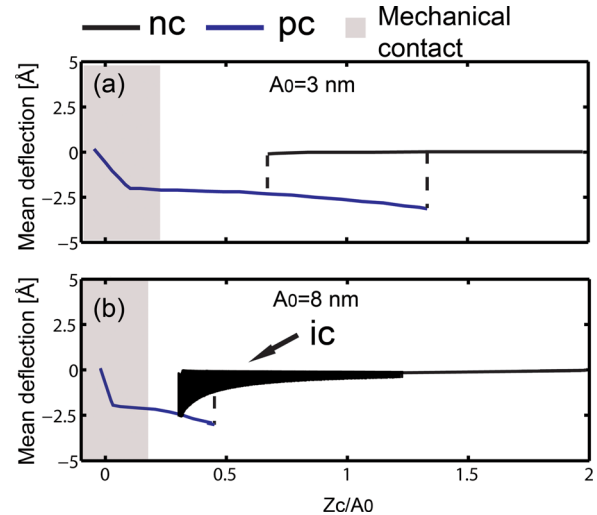


FIG. 4. (Color online) Simulated mean deflection (vertical axis) vs normalized separation (horizontal axis) for a free amplitude of (a) $A_0=3$ nm and (b) $A_0=8$ nm. The top figure corresponds to the simulated AD curve in Fig. 3(b) and the bottom one corresponds to that on Fig. 5(b). Mechanical contact only occurs at the smaller separations $z_c/A_0 \ll 1$. The mechanical contact regions are colored in gray but are of no interest here. Two oscillation amplitudes are observed in both curves. One (blue online) corresponds to oscillations where the tip is in perpetual contact (pc) with the water layers. There are also purely noncontact (nc) regions where the water layers are never perturbed (continuous black lines). The region in (b), indicated by an arrow and labeled ic, indicates that intermittent contact with the water layers occurs there. That is, the capillary bridge intermittently forms and ruptures. Simulation parameters as in Fig. 3.

is, the meniscus is never formed and ruptured during one cycle.

The phenomenon of $W_{CAP}=0$ is shown to lead to limit cycles with single period orbitals in Figs. 3(f)–3(h) respectively. In these, the vertical axis is the normalized instantaneous position of the tip z/A_0 (see Fig. 1) and the horizontal axis is the normalized instantaneous velocity \dot{z}/\dot{z}_{max} . Here, \dot{z}_{max} is the maximum instantaneous velocity of the tip when $z/A_0=1$, i.e., $\dot{z}_{max} \approx 5.1$ mm/s in this case. As, stated, for $z_c/A_0=0.5$, i.e., $z_c=1.5$ nm, the tip is in perpetual contact with the water and Fig. 3(f) shows that a single limit cycle with a single period orbital follows. Note that even when perpetual contact occurs, the solution is dynamic as it has larger than zero oscillation amplitude A . Also note that the amplitude A coincides in Figs. 3(f) to 3(h) with half the range of z and also coincides with the amplitudes in the frequency response in Figs. 3(c) to 3(e). For $z_c/A_0=1.0$ [Fig. 3(g)] two limit cycles are observed. The low amplitude branch (blue online) coincides with perpetual water contact. The high amplitude branch (continuous black lines) in the figure lies in the pure nc region. Moreover, this limit cycle coincides with the reported^{23,42–44} L -state or attractive regime. Figure 3(h) shows that with increasing oscillation amplitude A from $A \approx 1$ nm [Fig. 3(g)] to $A \approx 2.5$ nm [Fig. 3(h)], or equivalently in this case, at larger separations, from $z_c/A_0=1$ or $z_c=3$ nm [Fig. 3(g)] to $z_c/A_0=1.5$ or $z_c=4.5$ nm [Fig. 3(h)], there is a unique limit cycle, i.e., the L -state or attractive regime. This is a purely nc and single period orbital.

The above discussion has shown that provided perpetual water contact (blue online) or no water contact (continuous

black online) occurs during an oscillation cycle, there is only one frequency of oscillation in the response of the cantilever and limit cycles with single period orbitals follow. This is in a sense surprising since the physical phenomenon in one and the other scenario is different by involving liquid and air environments respectively. Nevertheless, some information can be found by observing the behavior of the mean deflection of the cantilever. In Fig. 4(a) the mean deflection curve corresponding to Fig. 3(b) is shown. Note how on extension and in the nc region (continuous black lines), zero or close to zero mean deflection follows. This is the response corresponding to the limit cycle shown in Figs. 3(g)–(h) in black lines, i.e., nc mode. Then, with decreasing separation, an abrupt step in negative deflection takes place. This step is indicated by dashed lines. Past this point the mean deflection is of the order of angstroms and corresponds to the limit cycle shown in Fig. 3(f). The tip is now in perpetual contact with the water. On retraction, there is hysteresis in the mean deflection corresponding to the existence of two limit cycles or attractors for a given separation. Nevertheless, no work is done by the capillary force during this hysteresis in other than the region for which the transition occurs (black dashed lines); see discussion above. Increasing the free amplitude to $A_0 = 8$ nm [Fig. 4(b)] results in the appearance of a region where the deflection does not take a single value any longer but has a range. This region is colored in black in Fig. 4(b) and corresponds to an intermittent contact region. That is, the tip is intermittently contacting the water layer and the capillary bridge is intermittently forming and rupturing. This implies that the minimum distance of approach d_{\min} has been reduced below d_{on} . According to simulations (data not shown) this is the typical behavior with increasing A_0 implying that d_{\min} decreases with increasing A_0 . Eventually, with increasing A_0 , a certain value of A_0 can be reached for which the repulsive regime sets and intermittent mechanical contact occurs throughout.^{38,40} Still, for this range of A_0 , Figs. 3, 4, and 5, mechanical contact does not occur above the point for which a local maximum in amplitude is observed [1 in Fig. 3(b)]. The local maximum in amplitude occurs slightly further away from the surface relative to the point for which the deflection changes slope (Fig. 4). When the deflection abruptly changes slope the oscillation amplitude is zero. The point at which mechanical contact occurs, past the local maximum in amplitude, is colored in gray in Fig. 4. This region always coincides with perpetual water contact. Thus that region is outside the scope of the perturbations predicted by Eq. (16). Moreover, here, we only discuss regions outside this mechanical contact region. Taking this into account we recall that d_{\min} decreases with increasing A_0 throughout.

From the stability expression Eq. (16), we note that decreasing values of d_{\min} lead to increasing instability since the capillary eventually forms and ruptures during an oscillation cycle, i.e., $d_{\min} < d_{\text{on}}$ and $d_{\max} > d_{\text{off}}$. Thus, since d_{\min} decreases with increasing A_0 , instability should increase with, for example, $A_0 = 8$ nm relative to $A_0 = 3$ nm as intermittent contact with the water occurs when $A_0 = 8$ nm as opposed to $A_0 = 3$ nm. By looking at Fig. 4, one could conclude that these predictions are in fact met in the simulations since the range of deflection values increases with A_0 in this way in the intermit-

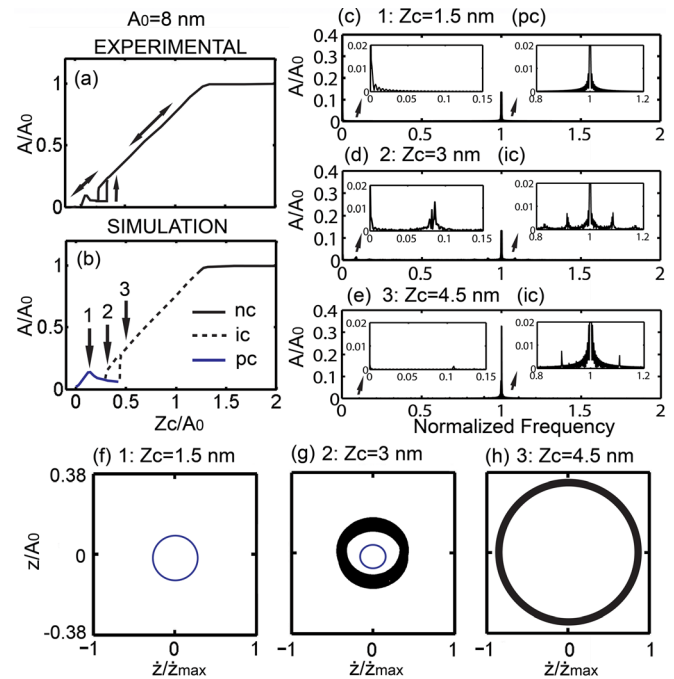


FIG. 5. (Color online) (a) Experimental amplitude distance (AD) curve as in Fig. 3(a) but where $A_0 = 8$ nm. The arrows indicate the extension and retraction path. (b) Simulation of a similar curve where the experimental characteristics are reproduced. The legends are as in Fig. 3. (c)–(e) FFTs obtained at three different separations z_c/A_0 as indicated by arrows in (b) and marked 1, 2, and 3 respectively as in Fig. 3. In (d) the FFT corresponds to the ic region in the curve. Now, subharmonics and frequencies close to the fundamental are excited where ic is predicted (see insets). The respective phase space diagrams displaying the limit cycles of the system at each separation are shown in (f)–(h), respectively as before. Where ic is predicted the limit cycles are multiple period orbitals. Again, as in for Fig. 3, the average force was monitored by simultaneously recording the phase lag where values above 90 degrees where also obtained here, i.e., attractive regime. Experimental parameters and simulation parameters as in Fig. 3 except for A_0 . Here $A_0 = 8$ nm.

tent water contact region. Also recall that Eq. (16) further predicts larger perturbations with decreasing oscillation amplitude A or A/A_0 . The range of deflection values is also observed to increase in Fig. 4(b) with decreasing A/A_0 . The limit cycles and frequency response in the case of intermittent contact are discussed next. These provide further evidence of the perturbations in oscillation amplitude induced by intermittent water contact. We also use the analytical expression Eq. (16) to compare the perturbations predicted by it with subharmonic excitation predicted by numerical simulations.

In Fig. 5 an AD curve for the case $A_0 = 8$ nm is shown experimentally [Fig. 5(a)] and with simulations [Fig. 5(b)]. In the simulated curve, a region where intermittent contact with the water occurs is shown (dashed line). This ic region coincides with the region with the large range in mean deflection in Fig. 4(b). Besides the intermittent contact region, this curve is otherwise similar to that in Fig. 3(b). The frequency spectrum at the same separations as before (Fig. 3) is shown in Figs. 5(c)–5(e). However, with this larger value of A_0 , the oscillation amplitude A has increased and the corresponding value of d_{\min} has decreased for the same separations thus inducing intermittent water contact in regions where no water contact occurred before in Fig. 3 where $A_0 = 3$ nm. The separations are (1) $z_c/A_0 = 0.19$

($z_c = 1.5$ nm), (2) $z_c/A_0 = 0.38$ ($z_c = 3$ nm), and (3) $z_c/A_0 = 0.56$ ($z_c = 4.5$ nm). At the smaller separations [Fig. 5(c)] no subharmonics or higher harmonics are excited. Again, this is a region of perpetual contact with the water [see region in Fig. 5(b)]. The meniscus is never formed and ruptured there during one cycle and $W_{CAP} = 0$ follows. Zero subharmonic excitation is then consistent with Eq. (16) and a unique limit cycle with a single period orbital follows [Fig. 5(f)]; the axes here have the same meaning and values as those in Fig. 3 the only difference being the value of A_0 where $A_0 = 3$ nm in Fig. 3 and $A_0 = 8$ nm in Fig. 5. At a slightly larger separation, there are two amplitude solutions, one where perpetual contact with the water occurs and another where intermittent contact follows. For the former, a similar situation is found in terms of frequency (not shown) as suggested by looking at its limit cycle in Fig. 5(g). Nevertheless, for the latter, subharmonics are excited [Fig. 5(d)]. These have amplitudes close to an angstrom and thus are, in principle, physically detectable. Furthermore, these subharmonics have typical frequencies that are approximately a tenth of the fundamental frequency [inset on the left in Fig. 5(d)]. Frequencies close to the fundamental are also excited [inset on the right in Fig. 5(d)]. The corresponding limit cycle [black region in Fig. 5(g)] covers an area of the phase space. This is in fact a multiple period orbital. The physical interpretation is that the intermittent contact with the water results in $W_{CAP} > 0$ and the water impacts are perturbing the oscillation amplitude. Moreover, according to Eq. (16), relatively large perturbations should follow when W_{CAP} is comparable to $1/2$ kA.² Thus, amplitude perturbations are predicted to decrease with increasing oscillation amplitude A in the intermittent contact region. In Fig. 5 this prediction is shown to be met in terms of frequency [Fig. 5(e)] and in terms of the area covered by the limit cycle [Fig. 5(h)]. In terms of the frequency, the subharmonics now have amplitudes of about 0.1 Å [inset on the left in Fig. 5(e)] and frequencies close to the fundamental have amplitudes close to half an angstrom [inset on the right in Fig. 5(e)]. Thus, by increasing the oscillation amplitude from $A/A_0 \approx 0.15$ ($A = 1.2$ nm) to $A/A_0 \approx 0.35$ ($A = 2.8$ nm) the area in the phase space has been reduced [c.f. black regions in Fig. 5(g) with 5(h)] and subharmonic excitation has been inhibited [c.f. insets on the left in Fig. 5(d) with 5(e)]. Our results further show (not all data shown) that both subharmonic excitation and multiple period orbitals are inhibited in the repulsive regime. Practically, this involves driving the cantilever with sufficiently large free amplitudes as to induce the onset of the repulsive regime where intermittent mechanical contact occurs.⁴⁰ These results can be compared to the predictions of Eq. (16) via the parameters controlling the perturbation P . For example, when $A = 1.2$ nm and with the parameters used in Fig. 5, we get; $W_{CAP} \approx 10$ eV (14), $W_{AD} \approx 170$ eV (15), $E_c \approx 157$ (17) eV and $P \approx 1.15$ (16). Since P is larger than 1, subharmonics should be excited agreeing with Fig. 5(d). Then, increasing the oscillation amplitude to $A = 2.8$ nm, $W_{CAP} \approx 10$ eV, $W_{AD} \approx 170$ eV, $E_c \approx 860$ eV, and $P \approx 0.21$. Again, this agrees with a reduction in the excitation of subharmonics as predicted numerically in Fig. 5(e). It is clear that further increasing the oscillation amplitude

will lead to $P \rightarrow 0$. This interpretation might provide a physical explanation to the success of AM AFM where instabilities were circumvented by sufficiently increasing the oscillation amplitude,⁴⁶ thus reducing the problems involved in tip trapping and adhesion.

The excitation of subharmonics can be understood from a physical point of view by looking at the wave forms of the amplitude and force (Fig. 6) for $A_0 = 3$ nm [Figs. 6(a)–6(b)] and for $A_0 = 8$ nm [Figs. 6(c)–6(d)], respectively. All these wave forms correspond to a separation of $z_c = 3$ nm and can be compared with the respective frequency and limit cycle in Figs. 3 and 5. First recall that for $A_0 = 3$ nm the interaction is pure non-contact and the water is never perturbed. Hence the wave form is an almost perfect sine wave [Fig. 6(a)]. Furthermore, the respective force profile shows a monotonous and periodic pattern [Fig. 6(b)]. When the free amplitude is increased to $A_0 = 8$ nm the wave form is observed to be modulated by lower frequencies [Fig. 6(c)]. Furthermore, the pattern is not monotonous (not all data shown). That is, the low frequency modulation lies in a range that goes from approximately $1/8$ to $1/13$ that of the fundamental in this case; note the peaks in frequency there [inset on the left in Fig. 5(d)]. The corresponding wave form for the net force now shows nonrepetitive peaks [Fig. 6(d)]. Physically, these results show that the tip is impacting the water during every 8–13 periods of fundamental oscillation. When the tip impacts the water layers [see arrows in Fig. 6(c)] the capillary does work against the elastic force of the spring, thus $W_{CAP} > 0$. At this point transients follow and there is a loss in oscillation amplitude A or stored energy E_c [see the wave form after the impact in Fig. 6(c)]. However, the water impacts are not repetitive in time; note the nonrepetitive behavior in both amplitude [Fig. 6(c)] and force [Fig. 6(d)] peaks. In summary, it is the intermittent impact during every several fundamental oscillations that excites subharmonics. Moreover, while the intermittent water impacts occur every several fundamental cycles, these still lie in the time-range of micro-seconds since f_0 here is 270 kHz; note water impacts taking place every $40\mu\text{s}$ approximately in Fig. 6. The prediction of subharmonics due to water impacts could thus be used to investigate processes such as nucleation time of water columns in the nanoscale for which a physical understanding is still emerging.^{24,27,29,47,48}

C. Consequences for apparent height

The prediction of a range of oscillation amplitudes due to the presence of subharmonics and multiple period orbitals also has implications in topography imaging in AM AFM. AM AFM is one of the most widely used forms of AFM to characterize the topography of surfaces.^{3,42,46} In Fig. 7 a simulation of the predictions of the apparent height of water layers is shown. These are the results of simulations where the difference in equilibrium distance z_c (see Fig. 1) between a surface with no water layers, i.e., $h = 0$ nm, and a surface with water layers of height h , i.e., $h = 0.6$ nm, is plotted in the vertical axis. This difference in z_c corresponds to the measured apparent height, or topography, in AM AFM. The horizontal axis corresponds to the normalized oscillation amplitude A/A_0 . The results are shown for three values of free amplitude. Initially, when the free amplitude is small, i.e.,

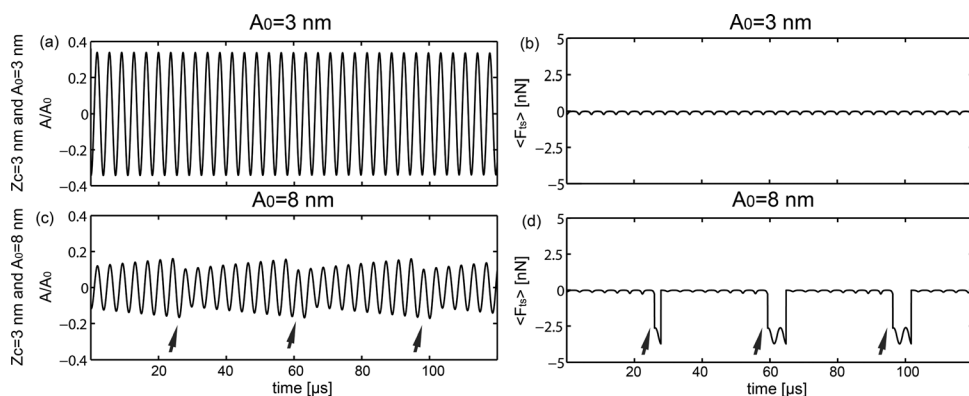


FIG. 6. Simulations. Wave forms for (a) the normalized oscillation amplitude A/A_0 and (b) the net tip-surface force F_{ts} at $z_c = 3$ nm for $A_0 = 3$ nm. This corresponds to the simulations in Fig. 3, and in particular Figs. 3(d) and 3(g) for non-contact oscillations. The oscillation amplitude is highly sinusoidal and the force form presents no peaks. When the free amplitude is increased to $A_0 = 8$ nm (c) and (d) the oscillation amplitude is modulated by lower frequencies and the F_{ts} wave form presents peaks corresponding to water impacts. The points at which the tip impacts the water layers are pointed at by arrows. Simulation parameters as in Fig. 3.

$A_0 = 3$ nm, and no water contact occurs, the predicted apparent height is 0.6 nm. Thus, in this pure nc mode the true height is recovered and a single value of height is obtained. These results correspond to the nc region in Fig. 3 where no subharmonics are excited [Figs. 3(d)–3(e)], the limit cycle is single period [black lines in Figs. 3(g)–3(h)], and where the wave form is purely harmonic [Fig. 6(a)]. When the free amplitude is increased to $A_0 = 8$ nm, the scenario corresponds to what is illustrated in Fig. 5 where intermittent contact with the water layers occurs [Fig. 5(b)] and the wave form shows no single frequency any longer [Figs. 5(d)–5(e) and Fig. 6(c)]. Furthermore, the phase space shows multiple period orbitals where the range in oscillation amplitude can be as large as several angstroms for a given separation [black region in Figs. 5(g)–5(h)]. The implications of intermittent contact in terms of apparent height are shown in Fig. 7 ($A_0 = 8$ nm). The figure shows that a range in apparent heights follows for a given oscillation amplitude A/A_0 . The apparent height however tends to increase relative to the true value. This is a consequence of the damping in energy during

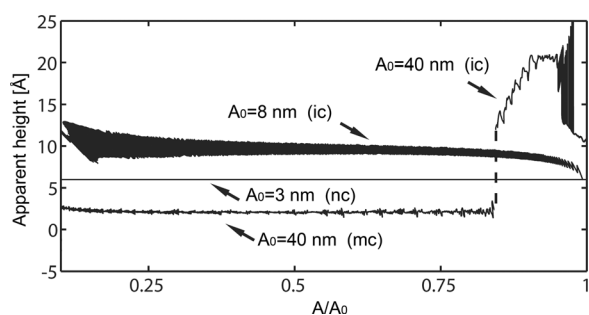


FIG. 7. Simulations for the apparent height of water patches as measured relative to dry regions. The water patches have been given a true height of 6 Å. The apparent height is given in angstrom units in the vertical axis vs normalized oscillation amplitude A/A_0 in the horizontal axis. The values are shown for three values of free amplitude. For the smaller free amplitude, i.e., $A_0 = 3$ nm, the measured apparent height is 6 Å and thus reproduces the true water height. This behavior corresponds to true noncontact (nc) where the water layers are never perturbed [Figs. 3 and 4(a) and 6(a)–(b)]. With increasing intermittent free amplitude ($A_0 = 8$ nm), intermittent contact with the water (ic) occurs. Mechanical contact still does not occur here but the apparent height increases relative to the true height. Further increasing the free amplitude to $A_0 = 40$ nm results in mechanical contact (mc). However, at large oscillation amplitudes the apparent height is predicted to dramatically increase.

water impacts where $W_{CAP} > 0$. For example, looking at the wave form [Fig. 6(c)], it follows that when an amplitude feedback reaches a given oscillation amplitude, the tip impacts the water layer and energy leaves the cantilever thus reducing the oscillation amplitude A or stored energy E_c (16). Then, after a few cycles, i.e., 8–13 [Fig. 6(c)], the amplitude increases again just to be damped once more in one or several cycles [see arrows in Fig. 6(c)] by water impacts. The result is that the set-point amplitude is never reached permanently and is, on average, smaller than the chosen set-point. Thus, an AM AFM will have to increase the separation to maintain the set-point and larger values of apparent height will then follow. Further increasing the free amplitude to $A_0 = 40$ nm induces a switch to the repulsive regime. This results in a decrease in the range of possible values of apparent height. In the figure, the region for which the repulsive regime is reached on both the dry ($h = 0$) and the wet ($h = 0.6$ nm) regions is indicated by an arrow and marked as mc, standing for intermittent mechanical contact (Fig. 7). At this point the apparent height is reduced to just 2–3 Å. In the simulations, we have allowed a monolayer of water molecules on the tip and the sample's surfaces [Fig. 2(b)].²¹ This has resulted in these 2–3 Å of apparent height in the simulations even in the repulsive regime. If no height is allowed to remain in this regime in the simulations, the predicted apparent height for the water layers is zero (data not shown). The requirement of leaving a finite value of height for the films on the tip's and sample's surfaces might be due to a solid-like nature of the first water bilayers adsorbed on the surface of BaF₂(111).³¹ Nevertheless, it could also be affected by the presence of ions,⁴⁹ hydration shells and the possible dynamics of squeeze-out of the water film. At this point, we believe that careful control experiments should be performed to establish the origins of this effect. The region termed intermittent contact or ic for $A_0 = 40$ nm in Fig. 7 consists of a region where the attractive regime is reached on the wet water patch, i.e., $h = 0.6$ nm, and the repulsive regime is reached on the dry water patch, i.e., $h = 0$ nm. This results in a further increase in apparent height relative to the values for $A_0 = 8$ nm where intermittent water contact occurs but intermittent mechanical contact does not. This extra step or increment in apparent height is a consequence of a gap in equilibrium separation between the attractive and the

repulsive regimes.^{50,51} The apparent height is shown to reach up to 20 Å. That is, over 3 times the true value of apparent height which is only 6 Å.

Experimental evidence of the range of values of the apparent height of water patches on surfaces using ambient AM AFM is shown in Fig. 8. The figure has been obtained on a BaF₂(111) surface for several values of free amplitude as in the simulations of Fig. 7. For clarity, the values given in Fig. 8(b) are the results obtained in a given experiment. Nevertheless, the experimental results here are general in that we have obtained similar results imaging several samples with several tips. The attractive and repulsive regimes have been monitored experimentally by recording the phase shift.⁴³ For the smaller values of free amplitude ($A_0 = 3$ nm) the apparent height is approximately constant with decreasing oscillation

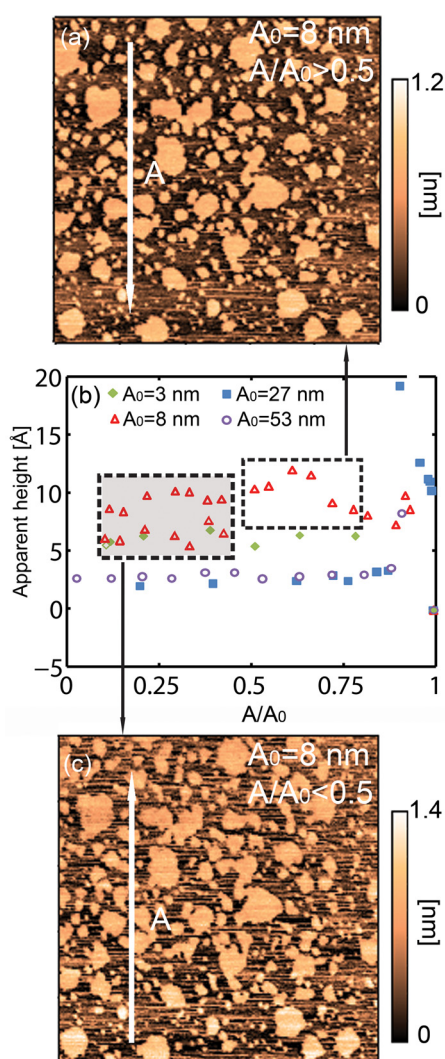


FIG. 8. (Color online) Experimental values of apparent height (vertical axis) vs normalized oscillation amplitude A/A_0 (horizontal axis) of water patches on a BaF₂(111) sample as shown in (b). The sample has wet and unwet regions (a) and (c). Thus, the measured apparent height corresponds to that of the wet regions relative to the dry regions. The working free amplitudes are 3 (rhombuses), 8 (triangles), 27 (squares), and 53 (circles) nm, respectively. The experimental parameters are the same as those in Figs. 3 and 4. The experimental behavior closely matches the predicted behavior in Fig. 7. The range of values for $A_0 = 8$ nm (triangles) can be attributed to intermittent water impacts perturbing the oscillation amplitude, particularly for the smallest oscillation amplitudes $A/A_0 < 0.5$ (c).

amplitude [rhombuses in Fig. 8(b)]. The apparent height is ~ 5 – 7 Å which is equivalent to one or two adsorbed water layers.³¹ The apparent height then increases with increasing free amplitude ($A_0 = 8$ nm, triangles). Significantly, the apparent height is larger with this free amplitude, i.e., relative to $A_0 = 3$ nm. Also, now, there is a range in values of apparent height, and especially, with decreasing oscillation amplitude in agreement with Eq. (16). A topography image for $A_0 = 8$ nm and for the largest values of oscillation amplitude $A/A_0 > 0.5$ is shown in Fig. 8(a). The oscillation amplitude A/A_0 has been decreased there from top to bottom. As A/A_0 decreases perturbations also increase in the image. Another image for $A/A_0 < 0.5$ is shown in Fig. 8(c). Now A/A_0 has been decreased from bottom to top. Perturbations are observed throughout. This behavior matches the predictions of the simulations in Fig. 7. Furthermore, when the free amplitude is increased to $A_0 = 27$ nm (squares), there is initially a severe step in measured apparent heights at the larger oscillation amplitudes, i.e., $A/A_0 > 0.8$. This corresponds to the attractive and the repulsive regimes being reached on the wet and dry surface regions, respectively. Again this behavior coincides with the predictions of Fig. 7. Finally, a switch to the repulsive regime on the wet region occurs and thus, the apparent height is dramatically reduced to 2–4 Å. Moreover, further increasing the free amplitude to $A_0 = 53$ nm (circles) results in repulsive imaging throughout but still, angstroms in apparent height remain. In Fig. 8(c) the perturbations imply that a range of heights can be measured for the water layers. This range is quantified by showing two triangles for each amplitude in Fig. 8(b) and for $A_0 = 8$ nm where most perturbations are observed (light gray colored region). The generality of these results is implied by the fact that for very small values of free amplitude, we typically obtained relatively stable values for the apparent height of the water layers with decreasing oscillation amplitude, A/A_0 . Then, increasing the free amplitude always resulted in the patterns described in Fig. 8 even if the particular value of free amplitude for which the repulsive regime is reached on the dry region, approximately 27 nm in the example in Fig. 8, might vary in different experiments. The variation of this value depends on the particular cantilever characteristics for a given sample.³⁸ Finally, it should be noted that a thorough experimental investigation of the consequences of capillary condensation on the excitation of higher harmonics should be conducted where relative humidity should be varied. These experiments could be performed with tips with different functionality, i.e., hydrophobic and hydrophilic coated,²³ and different levels of hydrophilicity of samples. Experimental subharmonic excitation should then be monitored by examining the frequencies of the experimental wave forms. The results we report here should provide significant fundamental understanding of the phenomena to experimentally interpret such data.

IV. CONCLUSION

The presence of water impacts at the nanoscale has been shown to lead to the excitation of subharmonics and multiple period orbitals. That is, there is a range of values of free amplitude, that typically lies below those for which the repulsive

regime is reached, for which subharmonic excitation is predicted to occur. At this point, the capillary bridge is predicted to intermittently form and rupture with frequencies below the fundamental. Thus, multiple period orbitals follow as a consequence of the water impacts where the fundamental oscillation amplitude is modulated by the frequency of impact. This frequency of impact typically lies, according to simulations, in the range of $\sim 1/8$ th to $1/13$ th that of the fundamental. Furthermore, water impacts could lead to subharmonic amplitudes in the order of angstroms which are, in any case, large enough to be detected. Further experimental investigations should establish whether subharmonic analysis could become a robust method to investigate the nucleation of water columns in the nanoscale with both spatial and temporal resolution. This, together with the versatility provided by the AFM to operate under a broad range of temperatures, pressures and working frequencies could open the door to the investigation of capillary condensation under different environmental conditions.

Furthermore, our analytic expression for the work done by the capillary force and adhesion during impacts and our interpretation of stability as the ratio between this work and the energy stored in the cantilever, have been shown to correlate with the findings in the simulations. This interpretation has been shown to hold provided the capillary bridge forms and ruptures during an oscillation cycle. Moreover, a limit cycle has been shown to appear under the conditions of perpetual contact with the water layers for which a single period orbital is predicted and where no subharmonics are excited. This is also consistent with the interpretation of perturbations in amplitude caused by the work done by the capillary force during the formation and rupture of the capillary bridge. That is, when the tip is in perpetual contact with the water, perturbations due to capillary forces in the vertical direction are either nonexistent or minimized.

We have also shown that the presence of subharmonics and multiple period orbitals could lead to errors in the measurement of apparent heights in AM AFM. Finally, we have shown that the measurements of apparent height of water layers when mechanical contact occurs are consistent with the predictions of simulations only if a finite height is allowed to remain on the surface during intermittent mechanical contact. Experimentally, we have found that about 2–4 Å of apparent height are measured.

ACKNOWLEDGMENTS

We acknowledge Maritsa Kissamitaki for the art work in this article and Neus Domingo for helping with the experimental setup. We would also like to thank Neil H. Thomson and Hugo K. Christenson for helpful discussions.

¹R. M. Brydson, C. Hammond, D. Mowbray, M. R. J. Gibbs, I. Todd, M. Grell, I. W. Hamley, M. Geoghegan, R. A. L. Jones, and G. J. Leggett, *Nanoscale Science and Technology* (Wiley, Chichester, 2005).

²N. Taniguchi, in *ICPE: International Conference on Production Engineering* (Tokyo, Japan 1974), p. 18.

³C. F. Quate, *Surf. Sci.* **299–300**, 980 (1994).

⁴C. Bustamante and D. Keller, *Phys. Today* **48**, 33 (1995).

⁵B. Bhushan, J. N. Israelachvili, and U. Landman, *Nature* **374**, 607 (1995).

⁶J. Israelachvili, *Intermolecular & Surface Forces*, 2nd ed. (Academic, New York, 1991).

⁷G. Binnig, C. F. Quate, and C. Gerber, *Phys. Rev. Lett.* **56**, 930 (1986).

⁸Y. Martin, C. C. Williams, and H. K. Wickramasinghe, *J. Appl. Phys.* **61**, 4723 (1987).

⁹A. L. Weisenhorn, P. Maivald, H. J. Butt, and P. K. Hansma, *Phys. Rev. B* **45**, 11226 (1992).

¹⁰A. I. Weisenhorn, P. K. Hansma, T. R. Albrecht, and C. F. Quate, *Appl. Phys. Lett.* **54**, 2651 (1989).

¹¹J. Tamayo and R. Garcia, *Langmuir* **12**, 4430 (1996).

¹²F. J. Giessibl, *Phys. Rev. B* **56**, 16010 (1997).

¹³R. Boisgard, D. Michel, and J. P. Aime, *Surf. Sci.* **401**, 199 (1998).

¹⁴J. P. Cleveland, B. Anczykowski, A. E. Schmid, and V. B. Elings, *Appl. Phys. Lett.* **72**, 2613 (1998).

¹⁵C. Loppacher, M. Bammerlin, F. Battiston, M. Guggisberg, D. Müller, H. R. Hidber, R. Lüthi, E. Meyer and H. J. Güntherodt, *Appl. Phys. A* **66**, S215 (1998).

¹⁶D. Sarid, J. P. Hunt, R. K. Workman, X. Yao, and C. A. Peterson, *Appl. Phys. A* **66**, 283 (1998).

¹⁷J. P. Aimé, R. Boisgard, L. Nony, and G. Couturier, *Phys. Rev. Lett.* **82**, 3388 (1999).

¹⁸H. Hölscher, U. D. Schwarz, and R. Wiesendanger, *Appl. Surf. Sci.* **140**, 344 (1999).

¹⁹M. Marth, D. Maier, and J. Honerkamp, *J. Appl. Phys.* **85**, 7030 (1999).

²⁰L. Nony, R. Boisgard, and J. P. Aime, *J. Chem. Phys.* **111**, 1615 (1999).

²¹A. Verdager, G. M. Sacha, H. Bluhm, and M. Salmeron, *Chem. Rev.* **106**, 1478 (2006).

²²N. Hashemi, H. Dankowicz, and M. R. Paul, *J. Appl. Phys.* **103**, 093512 (2008).

²³L. Zitzler, S. Herminghaus, and F. Mugele, *Phys. Rev. B* **66**, 155436 (2002).

²⁴E. Sahagun, P. Garcia-Mochales, G. M. Sacha, and J. J. Saenz, *Phys. Rev. Lett.* **98**, 176106 (2007).

²⁵M. Luna, J. Colchero, A. Gil, J. Gomez-Herrero, and A. M. Baro, *Appl. Surf. Sci.* **157**, 285 (2000).

²⁶M. Köber, E. Sahagún, P. García-Mochales, F. Briones, M. Luna, and J. J. Sáenz, *Small* **6**, 2725 (2010).

²⁷H. Choe, M.-H. Hong, Y. Seo, K. Lee, G. Kim, Y. Cho, J. Ihm, and W. Jhe, *Phys. Rev. Lett.* **95**, 187801 (2005).

²⁸H. K. Christenson and J. N. Israelachvili, *J. Colloid Interface Sci.* **117**, 576 (1987).

²⁹L. Bocquet, E. Charlaix, S. Ciliberto, and J. Crassous, *Nature* **396**, 735 (1998).

³⁰R. Szoszkiewicz and E. Riedo, *Phys. Rev. Lett.* **95**, 135502 (2003).

³¹A. Verdager, M. Cardellach, and J. Fraxedas, *J. Chem. Phys.* **129**, 174705 (2008).

³²A. French, *Vibrations and Waves* (Thomas Nelson and Sons Ltd., NY, 1981).

³³T. R. Rodríguez and R. García, *Appl. Phys. Lett.* **80**, 1646 (2002).

³⁴V. V. Yaminsky, *Colloids Surf., A* **159**, 181 (1999).

³⁵B. V. Derjaguin, V. Muller, and Y. Toporov, *J. Colloid Interface Sci.* **53**, 314 (1975).

³⁶H. C. Hamaker, *Physica* **4**, 1058 (1937).

³⁷S. Santos, Thesis, University of Leeds (2011).

³⁸S. Santos, V. Barcons, J. Font, and N. H. Thomson, *Nanotechnology* **21**, 225710 (2010).

³⁹S. Santos and N. H. Thomson, *Appl. Phys. Lett.* **98**, 013101 (2011).

⁴⁰R. Garcia and A. San Paulo, *Ultramicroscopy* **82**, 79 (2000).

⁴¹N. Martinez and R. Garcia, *Nanotechnology* **17**, S167 (2006).

⁴²R. Garcia and R. Perez, *Surf. Sci. Rep.* **47**, 197 (2002).

⁴³R. Garcia and A. San Paulo, *Phys. Rev. B* **60**, 4961 (1999).

⁴⁴R. Stark, G. Schitter, and A. Stemmer, *Phys. Rev. B* **68**, 0854011 (2003).

⁴⁵L. E. McNeil and M. Grimsditch, *J. Phys.: Condens. Matter* **5**, 1681 (1993).

⁴⁶Q. Zhong, D. Innls, K. Kjoller, and V. B. Elings, *Surf. Sci. Lett.* **290**, L688 (1993).

⁴⁷N. Maeda, J. N. Israelachvili, and M. M. Kohonen, *Proc. Natl. Acad. Sci. U.S.A.* **100**, 803 (2003).

⁴⁸U. Raviv, P. Laurat, and J. Klein, *Nature* **413**, 51 (2001).

⁴⁹T. E. Balmer, H. K. Christenson, N. D. Spencer, and M. Heuberger, *Langmuir* **24**, 1566 (2008).

⁵⁰P. Gleyzes, P. K. Kuo, and A. C. Boccarda, *Appl. Phys. Lett.* **58**, 2989 (1991).

⁵¹R. Garcia and A. San Paulo, *Phys. Rev. B* **61**, R13381 (2000).

⁵²See supplementary material at <http://dx.doi.org/10.1063/1.3663437> for details on the experimental set-up and a full description of the model used for the simulations.